

Supporting Information

Inductively heatable catalytic materials for the dehydrogenation of the liquid organic hydrogen carrier (LOHC) perhydrodibenzyltoluene

Markus Schörner^{#,1}, Thomas Solymosi^{#,1}, Theodor Razcka², Phillip Nathrath³, Nicolas Patrick Johner¹, Thomas Zimmermann^{2,4}, Karl Mandel^{2,4}, Peter Wasserscheid^{1,3,5}, Susanne Wintzheimer^{*,2,4}, Patrick Schühle^{*,3}

1 Helmholtz Institute Erlangen-Nürnberg for Renewable Energy (IEK-11), Forschungszentrum Jülich GmbH, Cauerstraße 1, 91058 Erlangen, Germany

2 Department of Chemistry and Pharmacy, Inorganic Chemistry, Friedrich-Alexander-Universität Erlangen-Nürnberg (FAU), Egerlandstraße 1, 91058 Erlangen, Germany

3 Friedrich-Alexander-Universität Erlangen-Nürnberg (FAU), Lehrstuhl für Chemische Reaktionstechnik (CRT), Egerlandstr. 3, 91058 Erlangen, Germany

4 Fraunhofer-Institute for Silicate Research ISC, Neunerplatz 2, 97082 Würzburg, Germany

5 Forschungszentrum Jülich GmbH, Institut für nachhaltige Wasserstoffwirtschaft (INW), Am Brainergy Park 4, 52428 Jülich, Germany

* Corresponding author: patrick.schuehle@fau.de, susanne.wintzheimer@fau.de

Experimental part

Materials

Steel beads S780 with a size fraction of 2.0 - 2.4 mm (Hasenfratz Ing. Büro Industrievertretungen GmbH, Sandstrahltechnik), γ -alumina beads (commercial ElemaxD102, Clariant AG), Fecralloy plates (Fe72.8/Cr22/Al5/Y0.1/Zr0.1, Goodfellow GmbH), Iron(II) sulfate heptahydrate ($\text{FeSO}_4 \cdot 7 \text{H}_2\text{O}$, 99.5%, Acros Organics), potassium nitrate (KNO_3 , 99+%, Acros Organics), potassium hydroxide (KOH, 90%, flakes, VWR International), boehmite powder (Disperal®, Sasol Germany GmbH), nitric acid (VWR International GmbH), γ -alumina powder (Puralox®, Sasol Germany GmbH and Catalox® (Sasol USA)), and platinum sulfite acid (15.3 wt-% Pt, abcr GmbH) were used without further purification unless stated otherwise.

Catalyst synthesis

Steel beads coated with γ -alumina and impregnated with Pt (Steel@Al₂O₃-Pt)

For the sol-gel-based coating dispersions, boehmite was stirred in water and nitric acid at 900 rpm for 10 min. Then, the γ -alumina powder was added, the dispersion was stirred for 6 h (Dispersion A, see Table S1 for details), and finally dispersed using an IKA Ultra Turrax Tube Drive S2 for further 30 min at a setting of 8. The inductively heatable steel beads were subsequently spray-coated with dispersion A on a tilted rotating sieve with intermediate drying until 11.89 wt%_{Al} was deposited. After calcination at 550 °C for 6 h, the coated beads were wet impregnated in an aqueous solution of platinum sulfite acid with a concentration of 0.05 g_{Pt} L⁻¹ using a rotary evaporator (at 323 K and stepwise reduction to 60 mbar) until all liquid was evaporated to reach an aimed loading of 0.3 wt%_{Pt}. Lastly, they were reduced at 440 °C in 10% H₂/N₂ for 2 h.

γ -Alumina beads spray-coated with a layer of γ -alumina-nanoparticles and IO supraparticles and impregnated with Pt (Al₂O₃@Al₂O₃-IO-Pt)

First, IO nanoparticles were synthesized based on a slightly modified oxidative precipitation method.¹⁻³ To minimize magnetic field induced effects the synthesis was carried out, as follows: FeSO₄·7 H₂O (10.01 g, 36.00 mmol) was dissolved in deionized water (1620 mL) and heated to boiling with the addition of nitrogen using an overhead stirrer and a heating mantle. In parallel, KOH (11.45 g, 183.6 mmol) and KNO₃ (25.48 g, 252.0 mmol) were dissolved in deionized water (180 mL) at 60 °C under nitrogen atmosphere. The iron oxide dispersion (2.5 wt%) was fed to the spray dryer (Büchi Labortechnik AG, B290 mini) at a pump speed of 10%, a flow rate of 40 l min⁻¹, and a suction rate of 75%. During spray drying (at an inlet temperature of 120 °C, resulting in an outlet temperature of 61 °C), the liquid was evaporated and the IO nanoparticles were assembled into larger micrometer-sized units, i.e., IO supraparticles.

For the sol-gel coating dispersion, boehmite was stirred in water and nitric acid at 900 rpm for 10 min. Then, the alumina powder was added, and the dispersion was stirred for 3.5 h (Dispersion B, see Table S1 for details). Before spray-coating, the IO supraparticles were added to B and dispersed using an IKA Ultra Turrax Tube Drive S2 for further 30 min at a setting of 8. γ -Alumina beads were spray-coated with dispersion B on a tilted rotating sieve with intermediate drying until 9 wt%_{Fe} was deposited on the pellets. The following calcination, Pt impregnation, and reduction were conducted in the same way as for Steel@Al-Pt, with a concentration of 0.05 g_{Pt} L⁻¹ to reach a loading of 0.3 wt%_{Pt}.

Steel plates coated with γ -alumina and impregnated with Pt (Plate@Al₂O₃-Pt):

The plate catalysts consisted of an inductively heatable iron substrate that was coated with a catalyst: FeCrAl-platelets of 5 x 5 mm were sandblasted, cleansed with acetone and spray-coated with dispersion A (see Table 1) in several layers with intermediate drying, resulting in an approximate support load of 11±0.5 mg per platelet. The following calcination, Pt impregnation, and reduction were conducted in the same way as for the beads, except that we impregnated the platelets using PSA solution with a concentration of 14.8 wt%Pt (STREM Chemicals) for 16 h.

From the Pt-concentration in the remaining impregnation solution measured via ICP-AES a loading of 3.78 wt%_{Pt} was calculated.

Table S1: Dispersion recipe for spray coating with A: Catalox® (Sasol USA) or B: Puralox® (Sasol Germany GmbH) as alumina powder, Disperal® (Sasol Germany GmbH) as boehmite powder, and 69% nitric acid (VWR International GmbH) for 100 g batches.

Dispersion	γ -alumina	Boehmite	IO supraparticles	H ₂ O	HNO ₃ (69%)	Stirring	Glycerol
A	23.76 wt%	2.64 wt%	0	70.4 wt%	2.58 wt%	6 h	0.6 wt%
B	13.6 wt%	6.1 wt%	6.21 wt%	73.2 wt%	0.92 wt%	4 h	0

Catalysts analysis

Inductively coupled plasma - optical emission spectrometry (ICP-OES) was used to analyze the Pt- and Fe-loading of the catalysts and was performed on a Ciros CCD (Spectro Analytical Instruments GmbH). For the catalyst plates and the steel beads, the coating was scratched off the metal plate for analysis. The solid samples were digested with concentrated HCl:HNO₃:HF in a 3:1:1 volumetric ratio, using microwave heating to 220 °C for 40 min. The instrument was calibrated for Pt (214.123 nm) with standard solutions of the elements before the analyses.

Nitrogen sorption measurements were performed on a NOVAtouch LX2 (AntonPaar) at 77 K. Before measurements, the samples were dried at 30 mbar and 115 °C for 16 h in a vacuum drying chamber (VO29, Mammert) and degassed at 350 °C for 12 h under vacuum.

Scanning electron microscopy (SEM) and energy-dispersive X-ray spectroscopy (EDX) were performed on a JSM F-100 (JEOL). Topographic analysis was conducted via secondary electron detection (15 kV accelerating voltage). The samples were sputtered with Au before SEM analysis. For the EDX characterization the accelerating voltage was kept at 15 kV. The catalyst samples were immobilized in an epoxy resin (Plano GmbH) and polished afterwards to reach a flat surface for SEM analysis. The catalyst samples were placed in a circular mould and fixated with shrink

tubing. A two component epoxy resin (Resine 603 supplied by Plano GmbH) was poured into the mould and put in an dessicator under vacuum. Next the sample was blow torched with a heat gun to remove any air bubbles. After 3 days the samples were demoulded, sanded and polished to 3000 grid (polishing diamant size 3 μm).

Induction heating experiments were performed using a high-frequency inverter SINUS 52 (Himmelwerk). For sample characterization outside a catalytic reactor, they were placed in the center of the copper coil, and magnetic fields up to 600 Oe and frequencies of 1419 KHz were applied at varying input voltages (1 to 45%). The magnetic field amplitudes for the various input voltage settings used in this manuscript were simulated in collaboration with the Himmelwerk company. The temperature was measured by using a CTlaser LTF pyrometer (Optris).

Dehydrogenation experiments

The catalysts were tested in both, an inductively and a thermally heated setup (see **Figure S1**). In both setups, the catalyst was placed in a glass test tube reactor, which was flushed with Argon and filled with H18-DBT. The system was then flushed with hydrogen and either placed in the center of an inductive heating coil (Himmelwerk) or into an oil bath to start of the experiment. The temperature in the reactor was measured with a type-K thermocouple (Rössel Messtechnik GmbH) and the released hydrogen flow was analyzed with a mass flow meter (Vögtlin Instruments GmbH, MFM). This way, the productivity of the catalyst and the degree of dehydrogenation (DoD) were continuously tracked. The mass flow meter was protected by a condensing unit and an active carbon filter. The following equations were used to calculate the DoD and the productivity from the measured hydrogen flow.

$$\text{DoD}(t) = \text{DoD}_0 + \frac{\int_0^t \dot{V}_{\text{N,H}_2} dt \cdot 0,0899 \frac{\text{g}_{\text{H}_2}}{\text{L}_{\text{N,H}_2}}}{n_{\text{H18-DBT}} \cdot 18,14 \frac{\text{g}_{\text{H}_2}}{\text{mol}_{\text{H18-DBT}}}} \quad (1)$$

With \dot{V}_{N,H_2} = measured hydrogen flow; DoD₀ = starting DoD at t = 0 min, in the herein used LOHC the starting DoD was 1%; $n_{H18-DBT}$ = molar amount of fully hydrogenated LOHC in the reactor at t = 0.

The mass related productivity P_m was calculated according to eq. 3 with m_{Pt} being the platinum mass used in the experiment.

$$P_m(t) = \frac{\dot{V}_{N,H_2}(t) \cdot 0,0899 \frac{g_{H_2}}{L_{N,H_2}}}{m_{Pt}} \quad (3)$$

With \dot{V}_{N,H_2} = measured hydrogen flow; m_{Pt} = mass of Pt in reactor.

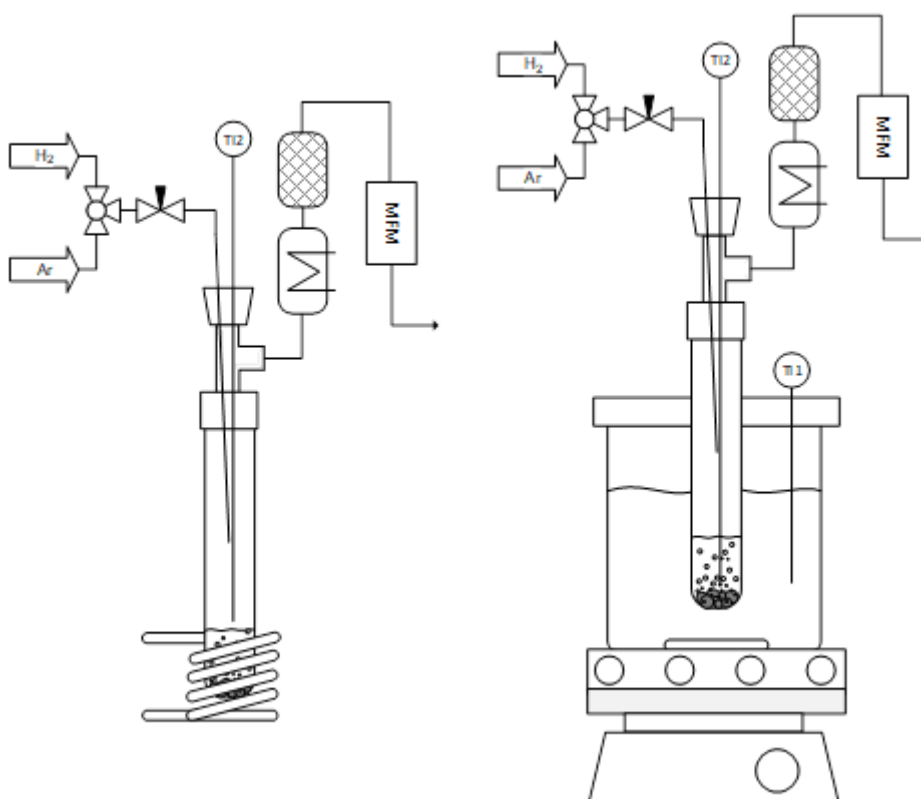


Figure S1: Reactor setup for inductively heated (left) and thermally heated (right) batch dehydrogenation of H18-DBT.

Liquid samples were taken at a DoD of 50%, 60%, and 70%. Those were used to verify the monitored DoD from the hydrogen production via NMR analysis according to literature^{4,5} and the high-boiler formation (30 μ L of sample, 0.7 mL of n-decane). High-boilers exhibit a higher boiling

point than dibenzyltoluene, thus eluate later from the GC column. This was determined by gas chromatography (Varian CP7531 column, Bruker 430-GC, GC) and all high boilers with a retention time between 33-45 min were considered as side products.

Results and discussion

Catalyst analysis

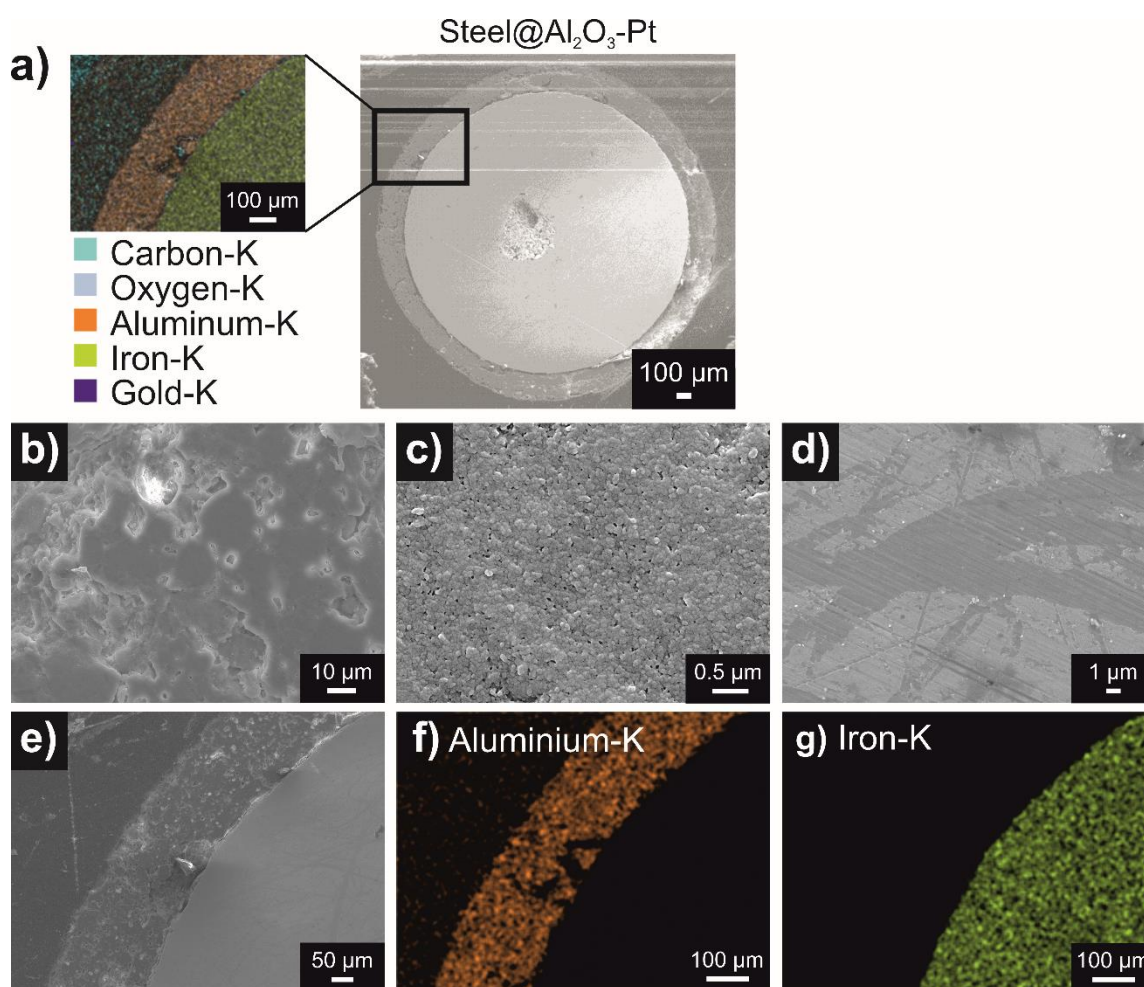


Figure S2. SEM and EDX cross section analysis of Steel@Al₂O₃-Pt. a) SEM and EDX overview micrograph of cross section of Steel@Al₂O₃-Pt with elemental mapping, b) Al₂O₃ outer shell with macroporous structure, c) Al₂O₃ outer shell with mesoporous structure, d) steel core surface, e) SEM overview micrograph of Al₂O₃ outer shell with steel core, f) EDX elemental mapping authenticating aluminium in outer shell, g) EDX elemental mapping authenticating iron in steel core.

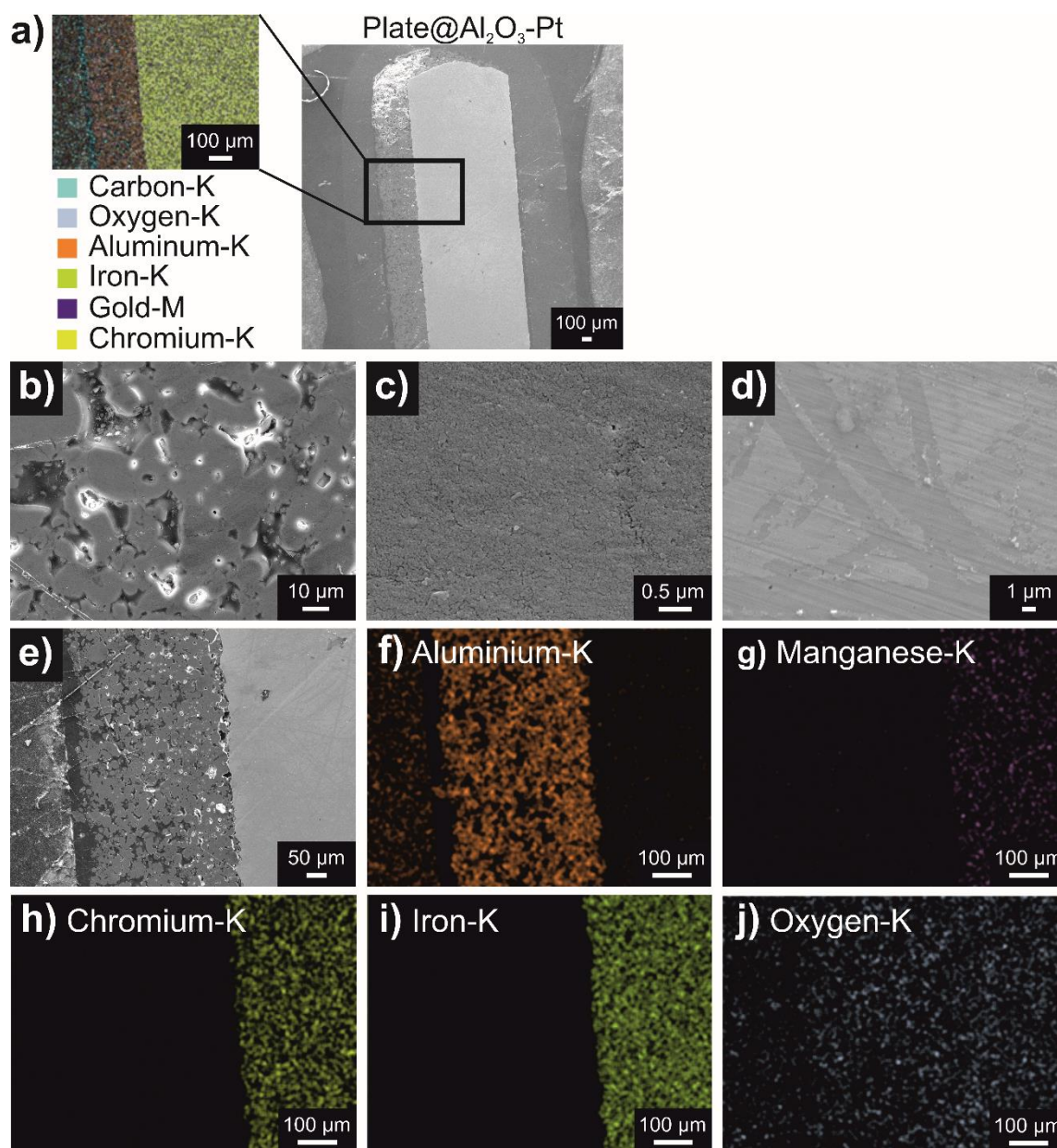


Figure S3. SEM and EDX cross section analysis of Plate@Al₂O₃-Pt. a) SEM and EDX overview micrograph of cross section of Plate@Al₂O₃-Pt with elemental mapping, b) Al₂O₃ outer shell with macroporous structure, c) Al₂O₃ outer shell with mesoporous structure, d) steel core surface, e) SEM overview micrograph of Al₂O₃ outer shell with steel core, f) EDX elemental mapping authenticating aluminium in outer shell, g) EDX elemental mapping authenticating manganese in steel core, h) EDX elemental mapping authenticating chromium in steel core, i) EDX elemental mapping authenticating iron in steel core, j) EDX elemental mapping authenticating oxygen.

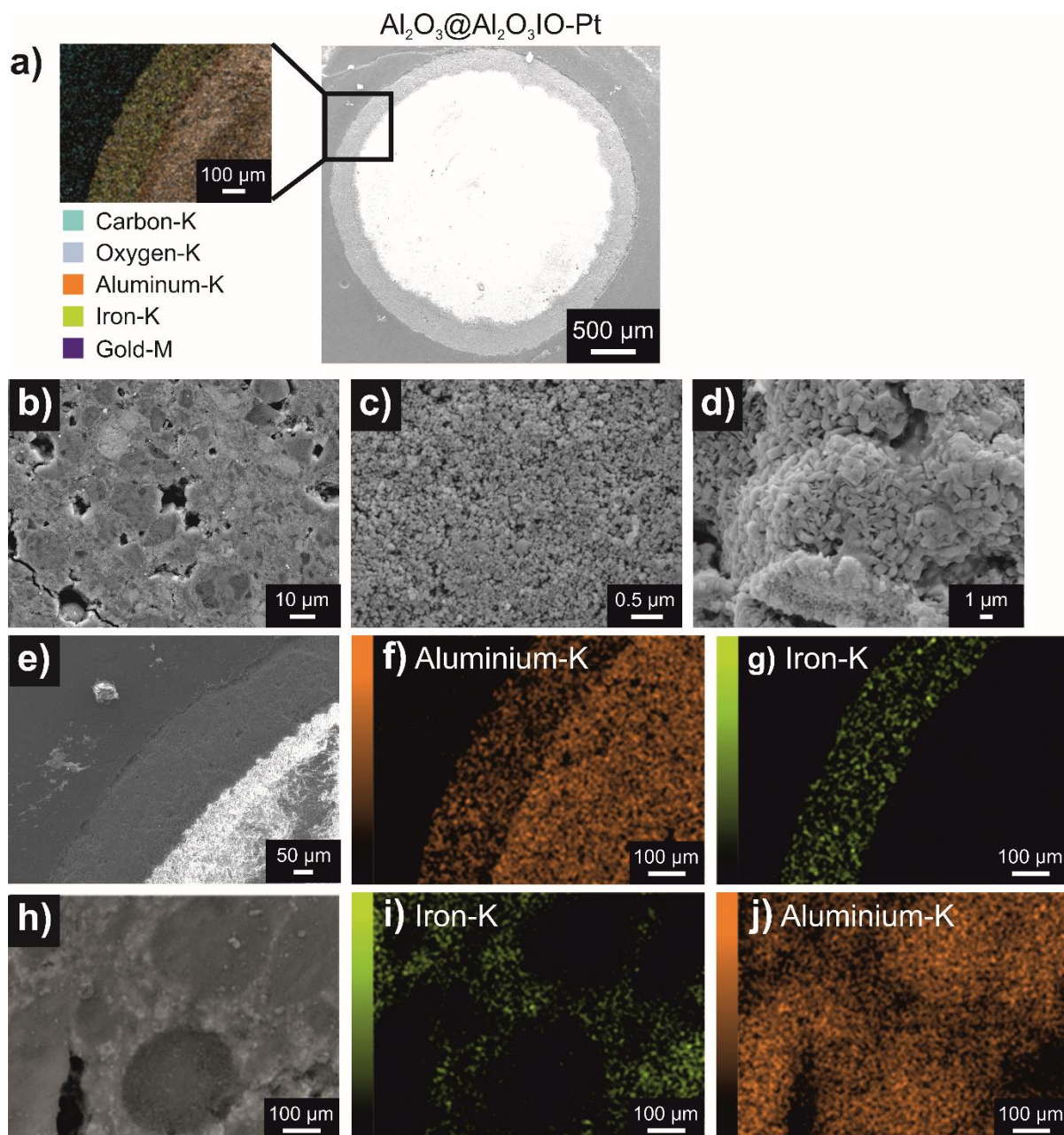


Figure S4. SEM and EDX cross section analysis of $\text{Al}_2\text{O}_3@\text{Al}_2\text{O}_3\text{IO-Pt}$. a) SEM and EDX overview micrograph of cross section of $\text{Al}_2\text{O}_3@\text{Al}_2\text{O}_3\text{IO-Pt}$ with elemental mapping, b) Al_2O_3 outer shell with macroporous structure, c) Al_2O_3 outer shell with mesoporous structure, d) porous aluminium oxide core structure, e) SEM overview micrograph of Al_2O_3 outer shell with aluminium oxide core, f) EDX elemental mapping authenticating aluminium in outer shell, g) EDX elemental mapping authenticating iron in steel core, h) zoomed in SEM image of outer shell structure i) EDX elemental mapping authenticating iron in zoomed in outer shell structure, j) EDX elemental mapping authenticating aluminium in zoomed in outer shell structure.

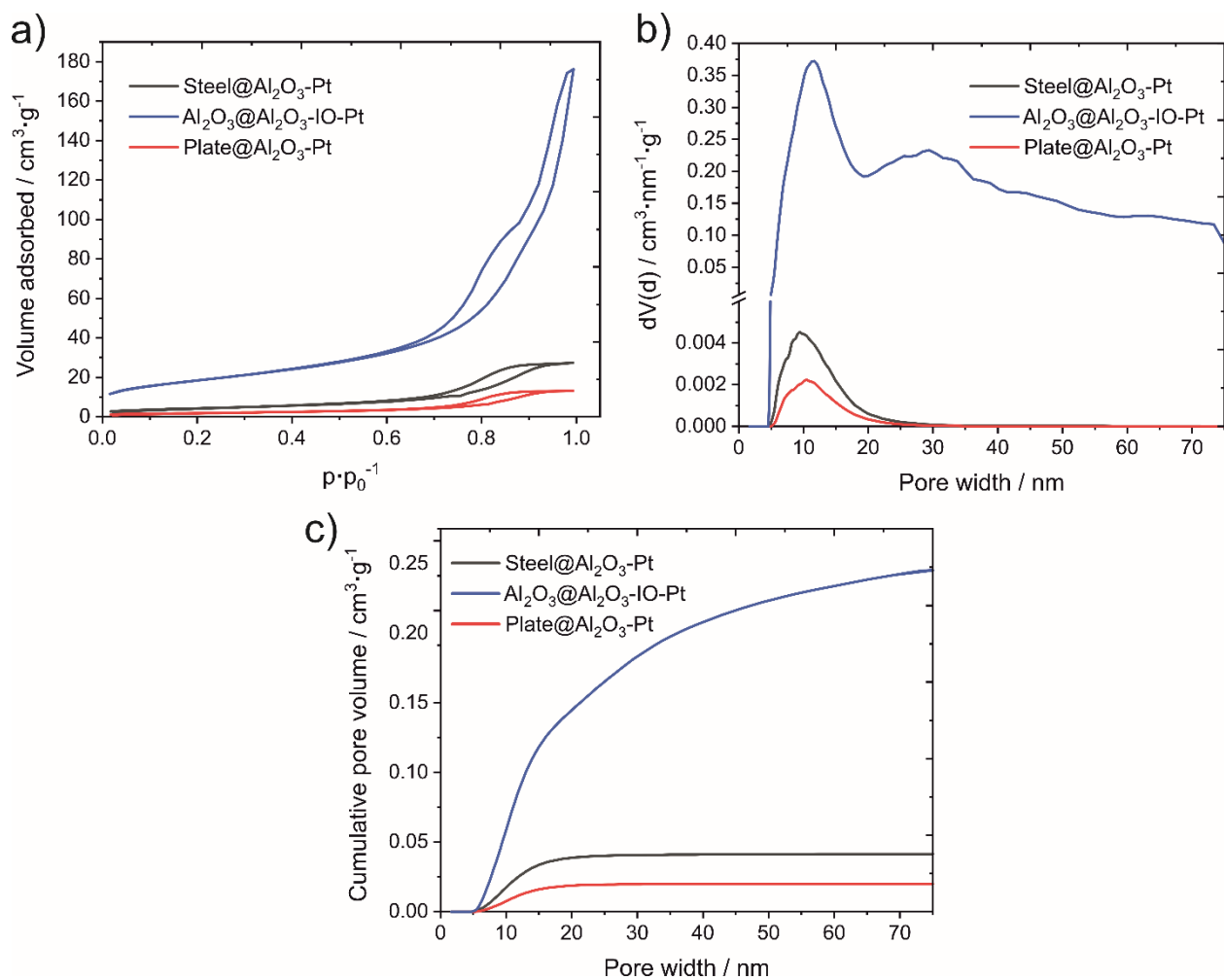


Figure S5. Pore system characterization of the three different catalysts via N₂ sorption at 77 K. a) N₂ isotherms, b) Pore size distribution obtained by NLDFT, c) Cumulative pore volume as a function of pore width.

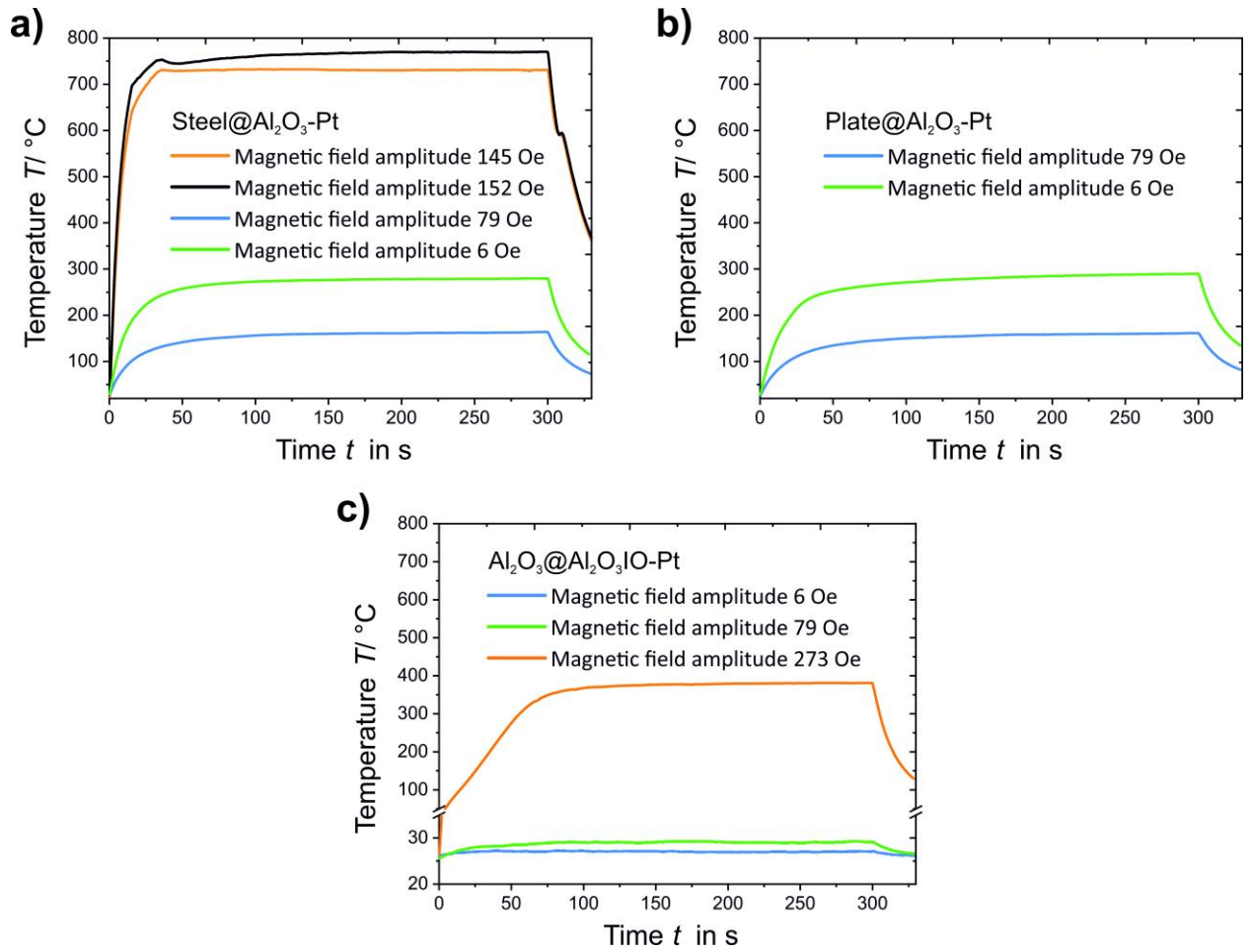


Figure S6. Inductive heating curves of a)Steel@Al₂O₃-Pt, b)Al₂O₃@Al₂O₃-IO-Pt and c)Plate@Al₂O₃-Pt using varying field strengths of 6, 79, 273 Oe field equal to U=1, 13 and 45% input voltage.

Dehydrogenation experiments Steel@Al₂O₃-Pt

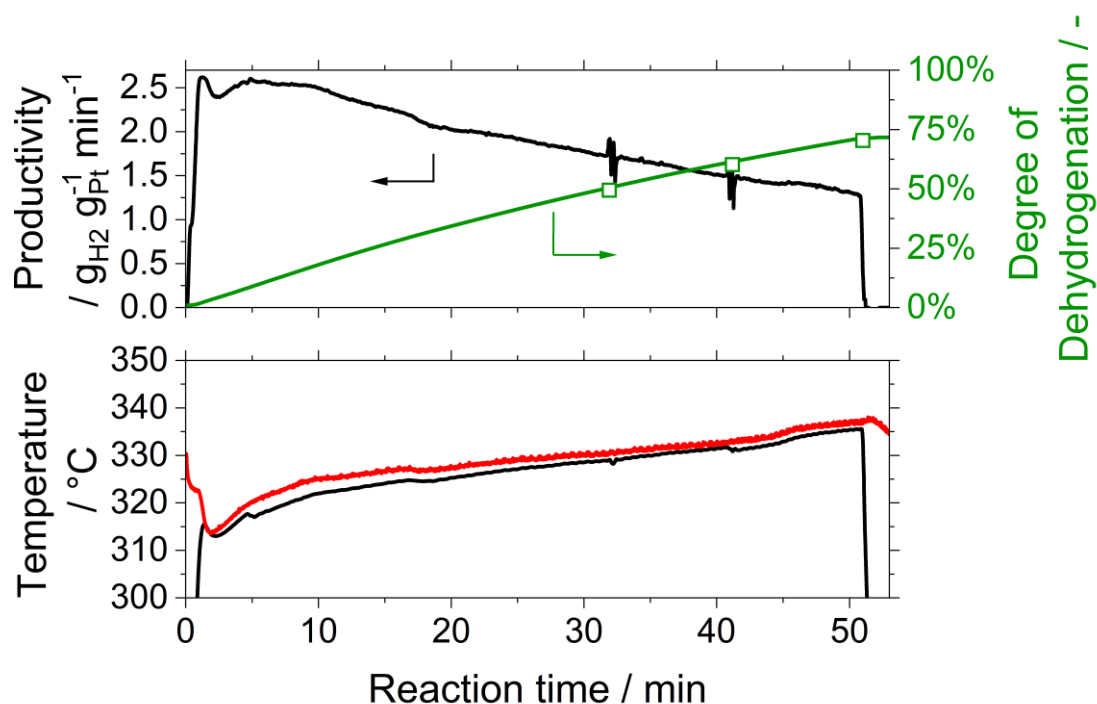


Figure S7. Productivity, DoD (top graph), and bulk as well as oil bath temperature (black as well as red curve, respectively, bottom graph) for the thermally heated batch dehydrogenation of H18-DBT depending on the reaction time using Steel@Al₂O₃-Pt. Liquid samples were taken at a DoD of 50%, 60%, and 70% for byproduct analysis and validation of the calculated DoD via hydrogen release (□). Reaction conditions: $w_{Pt} = 0.32$ wt-%, $m_{LOHC}:m_{Pt} = 2250$, $m_{cat} = 285.5$ mg,

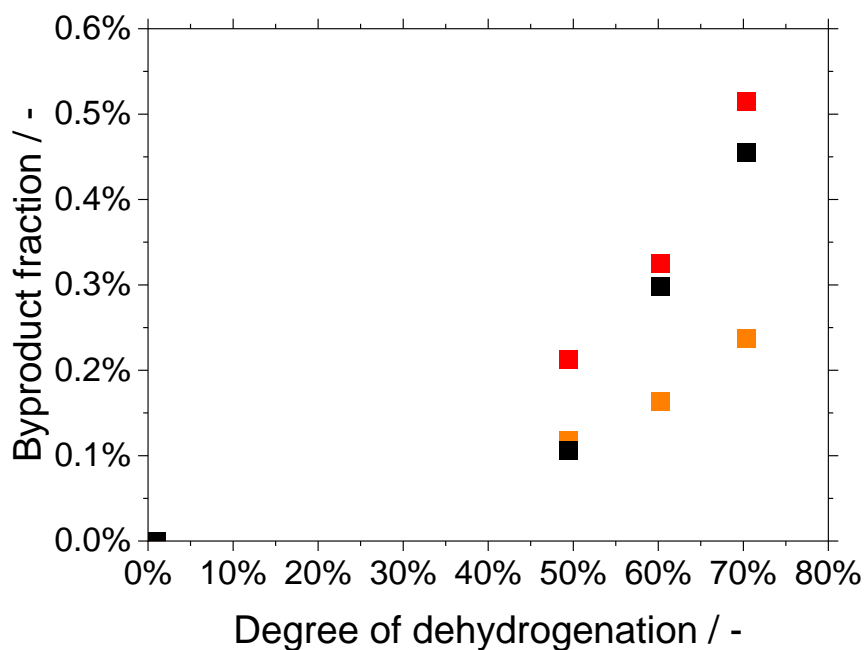


Figure S8: Fraction of formed byproducts during the dehydrogenation of H18-DBT in a thermally heated (red) and two inductively heated batch experiments (black and orange) using Steel@Al₂O₃-Pt. Reaction conditions: $w_{Pt} = 0.32$ wt-%, $m_{LOHC}:m_{Pt} = 2250$, $m_{cat,red} = 285.5$ mg, $m_{cat,black} = 288.1$ mg, $m_{cat,orange} = 280.6$ mg, Induction device settings orange: 145 Oe (magnetic field amplitude), Induction device settings black: 152 Oe (magnetic field amplitude).

Dehydrogenation experiments using Plate@Al₂O₃-Pt

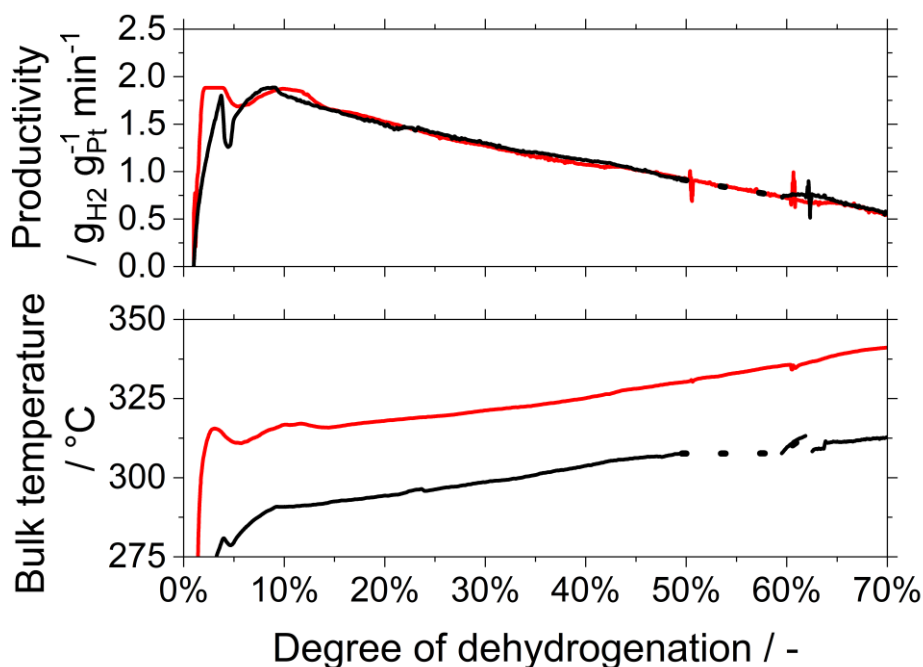


Figure S9: Productivity (top graph) and bulk temperature (bottom graph) for the dehydrogenation of H18-DBT in a thermally heated (red) and inductively heated (black) batch experiment using Plate@Al₂O₃-Pt as catalyst. Reaction conditions: $w_{Pt,layer} = 3.78$ wt-%, $m_{LOHC}:m_{Pt} = 1550$, $m_{cat,layer} = 32.7$ mg, Induction device settings: 79 Oe (magnetic field amplitude).

The top graph in Figure S9 shows the productivity for both, the inductive and the thermal heating experiment, using the Plate@Al₂O₃-Pt catalyst for H18-DBT dehydrogenation. In both cases, a maximal productivity of 1.9 g_{H2} g_{Pt}⁻¹ min⁻¹ was obtained at around 10% DoD. Afterwards the productivity continuously decreased with a further increase of DoD. At a DoD of 30% the productivity decreased by 32% to 1.3 g_{H2} g_{Pt}⁻¹ min⁻¹, at a DoD of 50% by 52% to 0.91 g_{H2} g_{Pt}⁻¹ min⁻¹, and at the final DoD of 70% by 71% to 0.56 g_{H2} g_{Pt}⁻¹ min⁻¹ compared to the productivity at a DoD of 10%. At a DoD of 10%, a temperature of 290.5 °C was measured in the bulk using inductive heating. During the experiment, the temperature increased continuously to 313.0 °C at a DoD of 70%. To mimic the measured productivity graph in the thermally heated experiment, the oil bath temperature was once again continuously increased throughout the experiment. As a result, also the bulk LOHC temperature increased continuously from 316.8 °C at a DoD of 10% to

341.4 °C at a DoD of 70%. A comparison of both bulk temperatures in Figure S9 bottom graph indicates that the bulk temperature during the inductive heating was 25 to 30 K lower than during thermal heating throughout the whole experiment.

Dehydrogenation experiments $\text{Al}_2\text{O}_3@/\text{Al}_2\text{O}_3\text{-IO-Pt}$

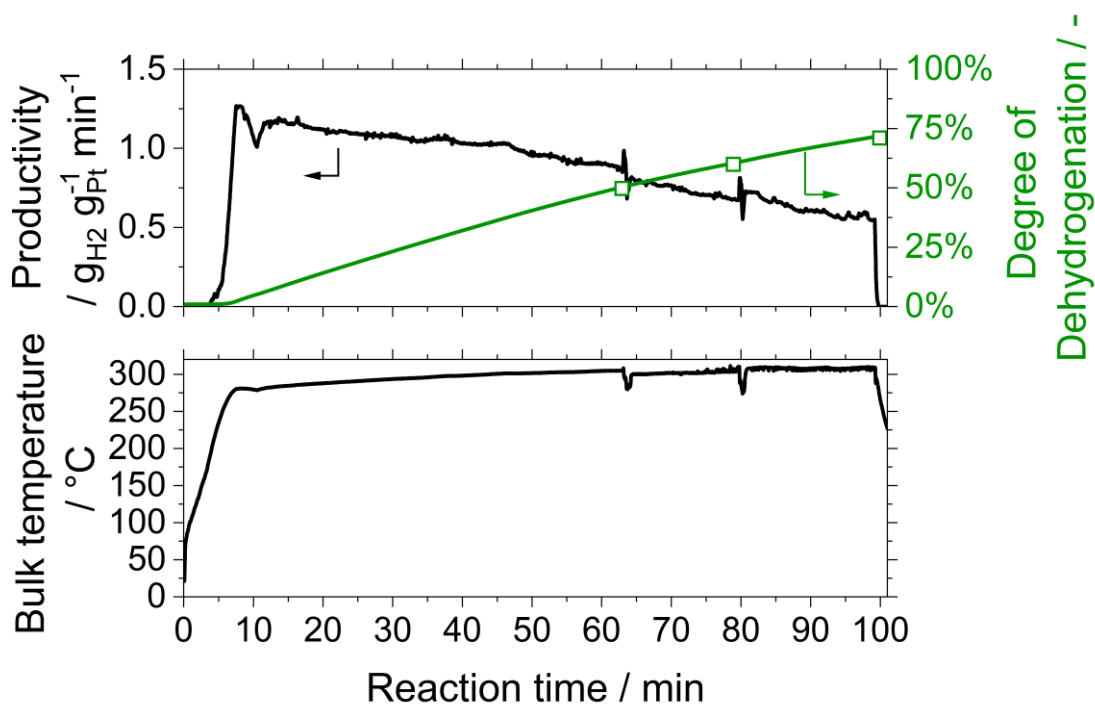


Figure S10. Productivity, DoD (top graph), and bulk temperature (bottom graph) for the inductively heated batch dehydrogenation of H18-DBT depending on the reaction time using $\text{Al}_2\text{O}_3@/\text{Al}_2\text{O}_3\text{-IO-Pt}$. Liquid samples were taken at a DoD of 50%, 60%, and 70% for byproduct analysis and validation of the calculated DoD via hydrogen release (\square). Reaction conditions: $w_{\text{Pt}} = 0.24$ wt-%, $m_{\text{LOHC}}:m_{\text{Pt}} = 1900$, $m_{\text{cat}} = 429.0$ mg, Induction device settings: 273 Oe (magnetic field amplitude).

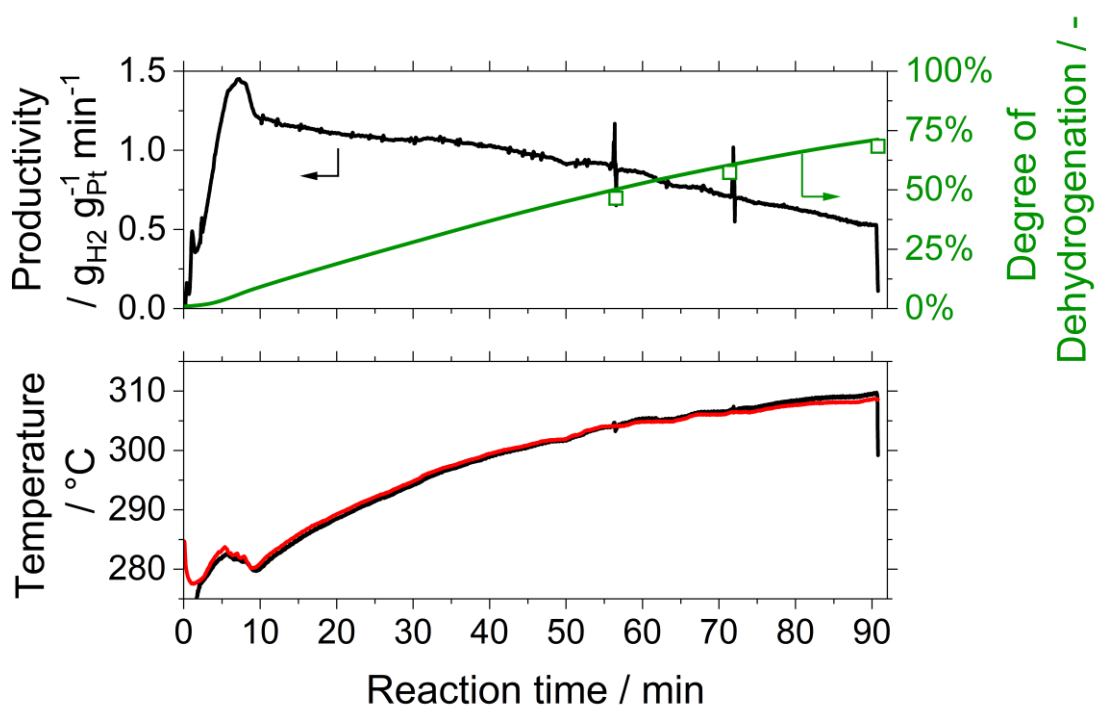


Figure S11. Productivity, DoD (top graph), and bulk as well as oil bath temperature (black as well as red curve, respectively, bottom graph) for the thermally heated batch dehydrogenation of H18-DBT depending on the reaction time using $\text{Al}_2\text{O}_3@\text{Al}_2\text{O}_3\text{-IO-Pt}$. Liquid samples were taken at a DoD of 50%, 60%, and 70% for byproduct analysis and validation of the calculated DoD via hydrogen release (\square). $w_{\text{Pt}} = 0.24$ wt-%, $m_{\text{LOHC}}:m_{\text{Pt}} = 1900$, $m_{\text{cat}} = 430.0$ mg.

The induction experiments were carried out first to determine the hydrogen productivity as a function of the DoD value. In the subsequent thermally heated experiment, the temperature of the oil bath was then adapted to reach a similar catalyst productivity as in the induction experiment. Since the $\text{Al}_2\text{O}_3@\text{Al}_2\text{O}_3\text{-IO-Pt}$ required a high current of the induction coil due to the hysteresis heating property of this catalyst, the magnetic field amplitude was set to 273 Oe. As a result, the utilized thermocouple heated up inductively as well. We found that the apparent temperature was 9.5 °C higher than without the induction (see **Figure S12**).

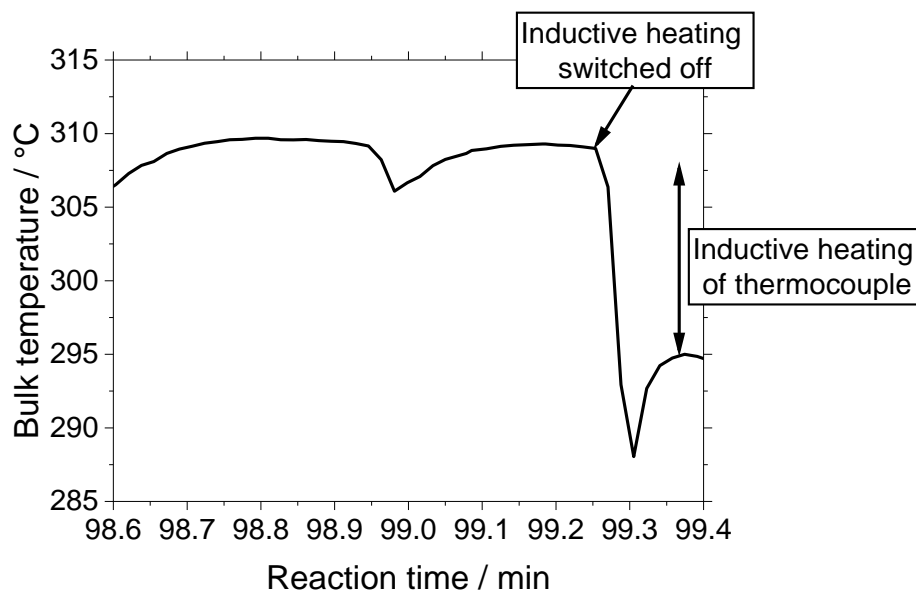


Figure S12. Unintended heating of the thermocouple by the induced magnetic field.

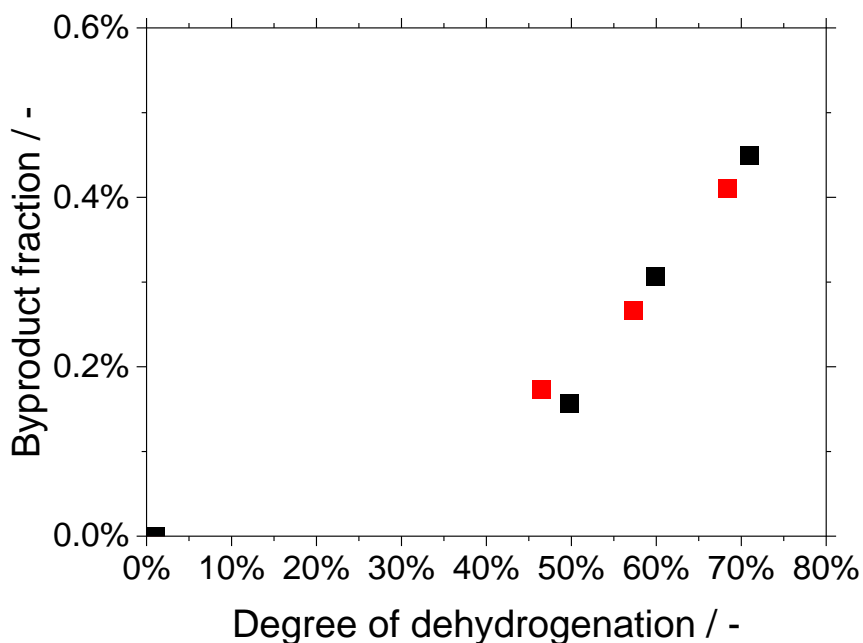


Figure S13: Fraction of formed byproducts for the dehydrogenation of H18-DBT depending on the degree of dehydrogenation in a thermally heated (black) and inductively heated (red) experiment using $\text{Al}_2\text{O}_3@/\text{Al}_2\text{O}_3\text{-IO-Pt}$. Reaction conditions: $w_{\text{Pt}} = 0.24 \text{ wt-\%}$, $m_{\text{LOHC}}:m_{\text{Pt}} = 1900$, $m_{\text{cat,red}} = 430.0 \text{ mg}$, $m_{\text{cat,black}} = 429.0 \text{ mg}$, Induction device settings: 273 Oe (magnetic field amplitude).

Recycle experiments

To show the stability of our catalysts we prepared another plate catalyst according to the details shown in the experimental section. The Pt-content in the spray-coated layer was determined by ICP-OES to 4.18 wt.-%. For the recycling of catalysts in the dehydrogenation of LOHCs

performed in a batch set-up is well-known from the literature that catalyst inhibition, which takes place during the cooldown, needs to be faced in the H18-DBT dehydrogenation.⁶ Overheating of the catalyst, before starting the recycle experiment is a proven strategy for easy reactivation.⁶

In the data shown in Figure S14, the induction device was set to 6 Oe in the first experiment (black). In the second run, the magnetic field was first set to 12 Oe and reduced after 2 min to 6 Oe as in the first run.

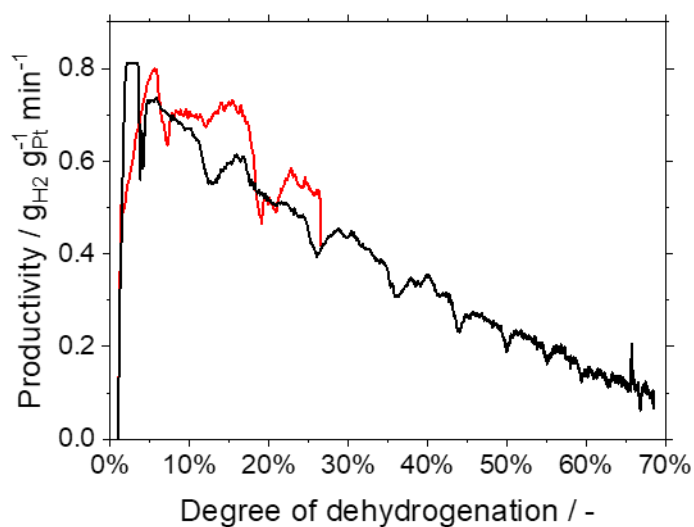


Figure S14: Hydrogen productivity for two consecutive runs (first run black, second run orange) of Plate@Al₂O₃-Pt as catalyst in the dehydrogenation of H18-DBT inductively heated batch experiment. The bulk temperature in the experiments reached a starting temperature of 275 °C and increased throughout the experiment slightly to 285 °C. Reaction conditions: $w_{Pt,layer} = 4.18$ wt-%, $m_{LOHC}:m_{Pt} = 842$, $m_{cat,layer} = 71.6$ mg, Induction device settings: 79 Oe (magnetic field amplitude).

SEM images of the spent Steel@Al₂O₃-Pt

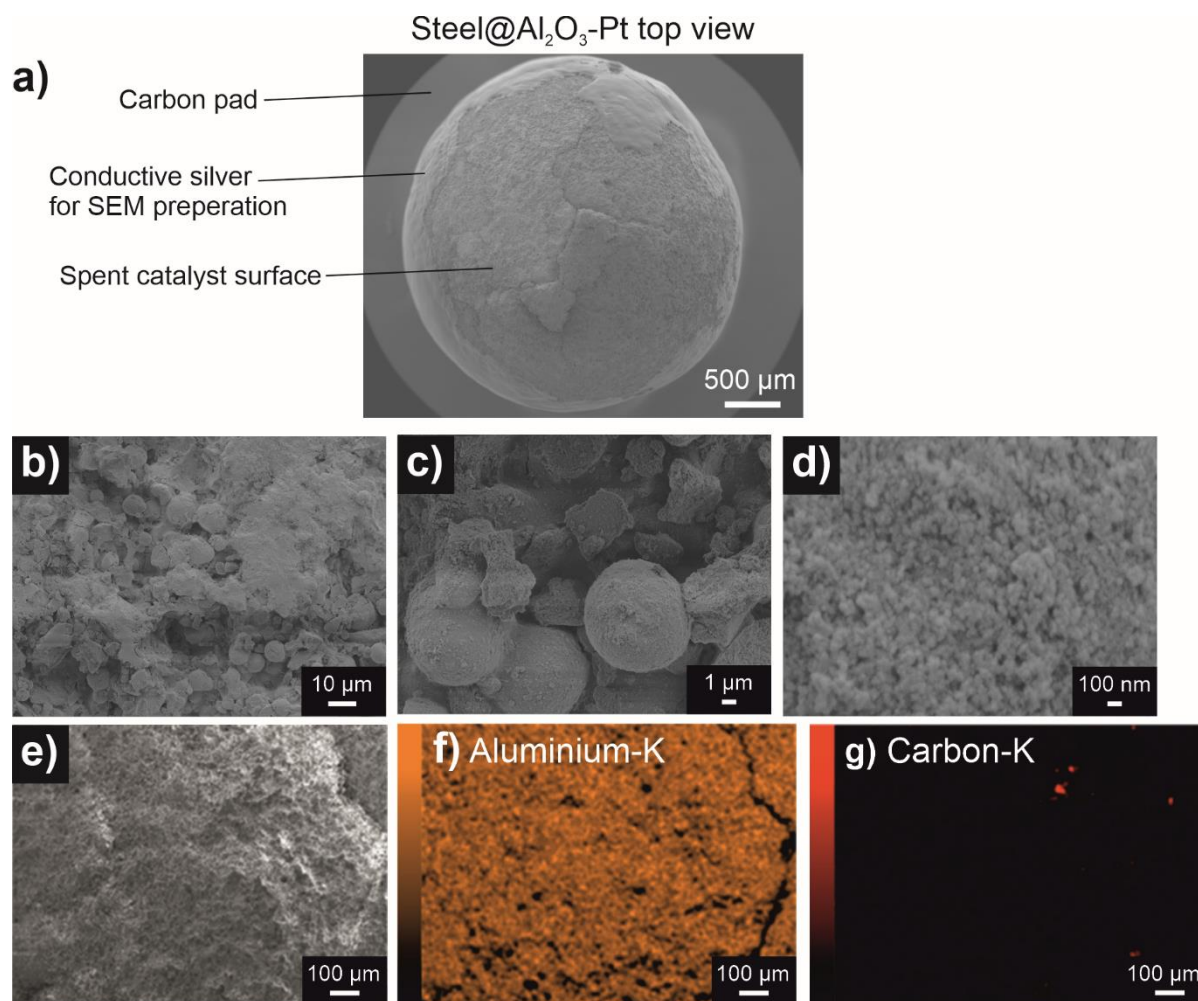


Figure S15. SEM and EDX top view analysis of Steel@Al₂O₃-Pt. a) SEM overview micrograph of top view of Steel@Al₂O₃-Pt with explanation, b) Al₂O₃ outer shell with macroporous structure, c) Al₂O₃ outer shell with macroporous structure zoomed in, d) Al₂O₃ outer shell with mesoporous structure, e) SEM overview micrograph of Al₂O₃ outer shell for EDX analysis, f) EDX elemental mapping authenticating aluminium in outer shell, g) EDX elemental mapping authenticating of formed carbon of the spent catalyst.

References

1. T. Granath, K. Mandel and P. Löbmann, *Particle & Particle Systems Characterization*, 2021, **38**.
2. F. Vereda, J. Vicente and R. Hidalgo-Alvarez, *Langmuir*, 2007, **23**, 3581-3589.
3. J. J. Brunner, M. Krumova, H. Colfen and E. V. Sturm Nee Rosseeva, *Beilstein J Nanotechnol*, 2019, **10**, 894-900.
4. G. Do, P. Preuster, R. Aslam, A. Bösmann, K. Müller, W. Arlt and P. Wasserscheid, *Reaction Chemistry & Engineering*, 2016, **1**, 313-320.
5. T. Solymosi, F. Auer, S. Dürr, P. Preuster and P. Wasserscheid, *International Journal of Hydrogen Energy*, 2021, **46**, 34797-34806.
6. T. Solymosi, M. Geisselbrecht, S. Mayer, M. Auer, P. Leicht, M. Terlinden, P. Malgaretti, A. Bosmann, P. Preuster, J. Harting, M. Thommes, N. Vogel and P. Wasserscheid, *Sci Adv*, 2022, **8**, eade3262.